Asian Journal of Chemistry; Vol. 25, No. 8 (2013), 4577-4582

ASIAN JOURNAL OF CHEMISTRY

http://dx.doi.org/10.14233/ajchem.2013.14203

Preparation of ZrO_2-C_{60} Nanocomposites Using Heat Treatment and Photocatalytic Degradation of Organic Dyes

BUM HWI CHO and WEON BAE KO*

Department of Chemisty, Sahmyook University, Seoul 139-742, South Korea

*Corresponding author: Fax: +82 2 9795318; Tel: +82 2 33991700; E-mail: kowb@syu.ac.kr

(*Received*: 18 June 2012; *Accepted*: 18 February 2013) AJC-13016

The ZrO_2 nanoparticles were synthesized by zirconia solution which is dissolved zirconyl chloride with distilled water and NH_4OH solution under microwave irradiation. The ZrO_2 and C_{60} nanocomposites were synthesized in an electric furnace at 700 ºC for 2 h. The heated ZrO_2-C_{60} nanocomposites were characterized by XRD, SEM and TEM. In addition, by using UV-visible spectroscopy, the heated ZrO_2-C_{60} nanocomposites were determinable as a catalyst in the photocatalytic degradation of organic dyes. The photocatalytic effect of the heated ZrO_2-C_{60} nanocomposites was confirmed as being compared with that of ZrO_2 nanoparticles after synthesis, heated ZrO_2 nanoparticles, unheated ZrO_2-C_{60} nanocomposites in various organic dyes such as methylene blue, methyl orange and rhodamine B under ultraviolet light at 254 nm.

Key Words: ZrO_2 nanoparticles, Fullerene[C_{60}], Methylene blue, Methyl orange, Rhodamine-B, ZrO_2-C_{60} nanocomposites, Photocatalytic degradation.

INTRODUCTION

Due to its unique properties, zirconia is one of the important ceramics. Zirconia has the excellent combination of electrical, mechanical, optical and thermal properties and is able to be a good choice for applications such as structural material, thermal barrier coating, solid oxide fuel cell electrolytes and semiconductor material[1-4]. In addition, zirconia has stable photochemical properties so it is directly applicable to photonics[1,5]. Moreover, because of unique amphoteric characteristics and redox properties, zirconia can be appropriate for a catalyst or a catalyst support[1,6].

In the past decade, numerous techniques have been developed for the synthesis of nano-sized ZrO_2, whereas the polyol process has been largely studied and well adopted[7-10]. Zirconia shows several crystalline variations depending on temperature; at the temperatures below 1172 ºC, monoclinic is stable; at the temperature range 1172-2347 ºC, tetragonal is stable; above 2347 ºC, cubic is stable; and rhombic is stable at a high pressure. However, at low temperatures between 550 and 750 ºC, tetragonal and cubic zirconia is able to be arranged in the forms of highly dispersed metastable phases. In area of ceramic and catalytic applications of zirconia, the martensitic conversion from the tetragonal to the monoclinic structure has huge importance. Generally, the tetragonal phase of zirconia is favorably formed corresponding to the monoclinic phase during the crystallization temperature, most of amorphous hydrous zirconia. For that reason, upon increasing calcination temperature, most of amorphous zirconia precursors transform to the tetragonal phase firstly and then convert to the monoclinic phase at higher temperature up to 600 ºC. Above approximately 800 ºC, conversion is completed[11-14].

C_{60} Fullerene is a promising material. It is a well-established singlet oxygen sensitizer used in the outline of organic synthesis photooxidations[15-19] and absorbs strongly in the ultraviolet and moderately in the visible region of the spectrum[15,20-23]. As C_{60} is irradiated with UV-visible radiation, it is excited from the ground state to a short-lived singlet excited state (*ca.* 1.2 ns)[15,24] which go through rapid intersystem crossing at a rate of 5.0×10^8 s^{-1} to a lower lying triplet state ($^3C_{60}$*) with a long left time (> 40 μs)[15,25,26]. More significantly, photoexcited fullerenes are also excellent electron acceptors capable of accepting six electrons[15,27,28].

Nanosized metal particles, semiconductors and oxides have attracted a great deal of attention in materials science because of their specific physical and chemical properties based on quantum size effects[29-32]. Transition metal oxides, such as copper, iron, nickel, cobalt and zinc, ranging from micrometer to nanometer particle sizes have been widely studied for applications in photonics, piezoelectrics, magnetic storage media, solar energy transformation, electronics, semiconductors, varistors, electrical and optical switching devices, batteries,

sensors, catalysis, drug delivery systems and separation techniques[29,33-40].

Photocatalytic materials take part in a very essential role for selective organic transformations in a cost-effectively and environmentally friendly. Many of these catalytic systems are operated in aromatic or halogenated hydrocarbon solvents, which are environmentally detrimental. Moreover, most of them suffer from several restrictions; being usually only effective with reactive alcohols or involving high pressures and/or temperature and high catalyst loading[41-44].

In particular, heterogeneous photocatalysis is an efficient technique to remove organic contaminants in water[45-48].

EXPERIMENTAL

C_{60} was purchased from Tokyo Chemical Industry Co., Ltd. Tetrahydrofuran, NH_4OH and ethanol were obtained from Samchun Chemicals. The zirconyl chloride octahydrate and organic dyes (methylene blue, methyl orange and rhodamine-B) were supplied by Sigma-Aldrich.

An electric furnace (Ajeon Heating Industry Co., Ltd.) was used to heat the sample. A UV lamp (8 W, 365 nm, 77202 Marne La Valee-cedex 1 France) was used as the ultraviolet light irradiation source.

The surfaces of the unheated ZrO_2 particles, heated ZrO_2 particles, unheated ZrO_2-C_{60} nanocomposites and heated ZrO_2-C_{60} nanocomposites were observed by SEM (Hitachi S4700) at an accelerating voltage of 0.5-15 kV. The morphology and crystallite size of the samples were examined by TEM (JEOL Ltd, JEM-2010) at an acceleration voltage of 200 kV. The structures of the nanomaterials were examined by XRD (Rigaku, Rigaku DMAX PSPC MDG 2000). UV-visible spectra of the samples were performed using a UV-visible spectrophotometer (Shimazu UV -1601PC).

Microwave irradiation was carried out in multimode with continuous heating at full power in a domestic oven (2450 MHz, 700W).

Synthesis

Synthesis of ZrO_2 nanoparticles: 0.1 M zirconyl chloride was dissolved in distilled water, then adding NH_4OH until the pH was reached from 7 to 11. During on stirring, it was changed solution to gel. The gel state sample was washed by ethanol for 5 times with centrifuge. After drying at the room temperature, the sample was heated under the microwave condition for 3-5 min.

Synthesis of ZrO_2-C_{60} nanocomposites: In a typical experiment, the prepared ZrO_2 and prepared C_{60} nanoparticles were mixed as the molar ratio of 5:1. The mixture was dissolved in 10 mL of THF with stirring to produce the ZrO_2-C_{60} nanocomposites. The mixture was then dried at room temperature. After drying the nanocomposites, they were heated in an electric furnace at 700 ºC for 2 h.

Degradation of organic dyes with nanocomposites: To examine the photocatalytic activity of unheated ZrO_2 nanoparticles, heated ZrO_2 nanoparticles, unheated ZrO_2-C_{60} nanocomposites and heated ZrO_2-C_{60} nanocomposites were examined using some organic dyes, methylene blue (MB), methyl orange (MO) and rodamine-B (RhB). 10 mg of each nanomaterial was dispersed in 10 mL of water containing 0.01 mM of each organic dye solution. All the mixture solutions were irradiated with ultra-violet light at 254 nm for 20 min. The organic dyes degraded by each nanomaterial under ultraviolet light were characterized by UV-VIS spectrophotometer.

RESULTS AND DISCUSSION

Fig. 1 showed SEM images of unheated ZrO_2 nanoparticles, heated ZrO_2 nanoparticles, unheated ZrO_2-C_{60} nanocomposites and heated ZrO_2-C_{60} nanocomposites. Fig. 1(a-b) showed SEM images of unheated ZrO_2 nanoparticles and heated ZrO_2 nanoparticles, respectively. Compared unheated ZrO_2 nanoparticles with heated ZrO_2 nanoparticles, the shape of heated ZrO_2 nanoparticles was more agglomerated figure than the shape of unheated ZrO_2 nanoparticles (Fig. 1(a-b)). Fig. 1(c-d) showed SEM images of unheated ZrO_2-C_{60} nanocomposites and heated ZrO_2-C_{60} nanocomposites, orderly. ZrO_2 nanoparticles of both unheated ZrO_2-C_{60} nanocomposites and heated ZrO_2-C_{60} nanocomposites were located above C_{60} nanoparticles. After heat treatment, C_{60} nanoparticles were broken into small parts in heated ZrO_2-C_{60} nanocompsoites and also the shape of heated ZrO_2-C_{60} nanocomposites had a porous surface.

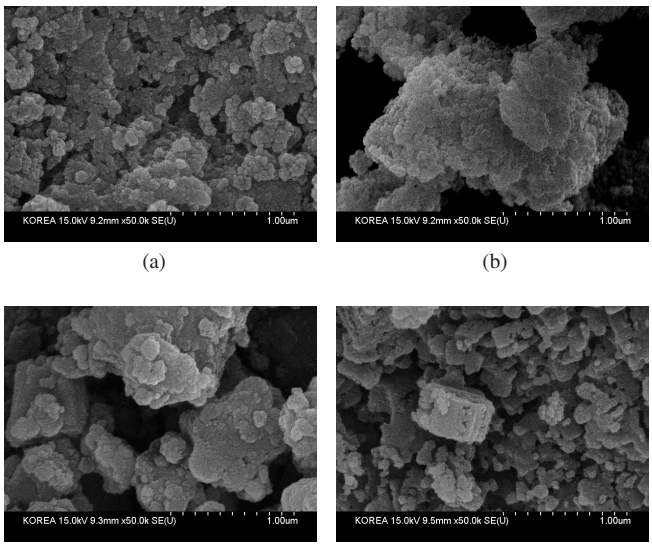

(a) (b) (c) (d)

Fig. 1. SEM images of (a) unheated ZrO_2 nanoparticles, (b) heated ZrO_2 nanoparticles, (c) unheated ZrO_2-C_{60} nanocomposites, and (d) heated ZrO_2-C_{60} nanocomposites

Fig. 2 showed TEM images of the unheated ZrO_2 nanoparticles, heated ZrO_2 nanoparticles, unheated ZrO_2-C_{60} nanocomposites and heated ZrO_2-C_{60} nanocomposites. Above all, compared unheated ZrO_2 nanoparticles [Fig. 2(a)] with heated ZrO_2 nanoparticles [Fig. 2(b)], heated ZrO_2 nanoparticles showed more crystallinity than unheated ZrO_2 nanoparticles because heated ZrO_2 nanoparticles were undergone by heat treatment. In addition, heated ZrO_2 nanoparticles had porous surfaces. After that, contrasted unheated ZrO_2-C_{60} nanocomposites [Fig. 2(c)] to heated ZrO_2-C_{60} nanocomposites [Fig. 2(d)], because of the heat treatment, C_{60} in heated ZrO_2-C_{60} nanocomposites was broken into smaller particles. As a consequence, heated ZrO_2-C_{60} nanocomposites had higher surface area than unheated ZrO_2-C_{60} nanocomposites. As a result, heated nanomaterials which heated ZrO_2 nanoparticles and

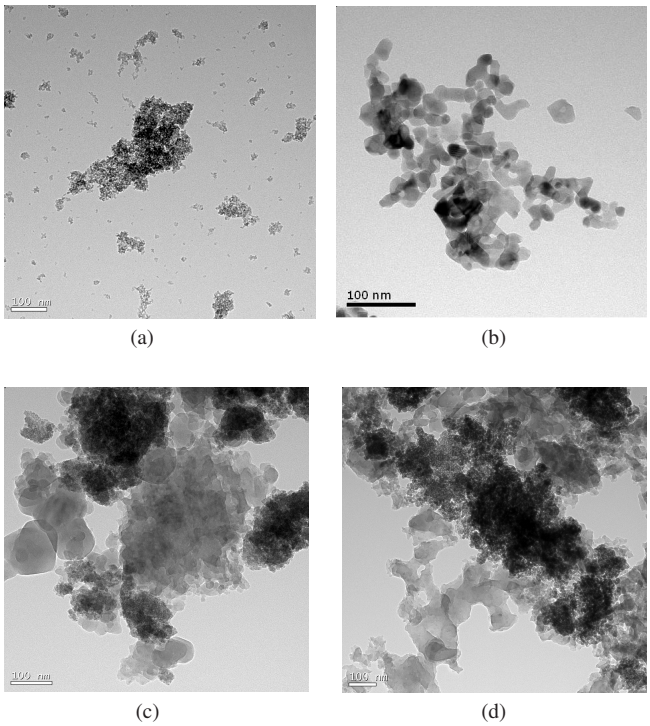

Fig. 2. TEM images of (a) unheated ZrO_2 nanoparticles, (b) heated ZrO_2 nanoparticles, (c) unheated ZrO_2-C_{60} nanocomposites, and (d) heated ZrO_2-C_{60} nanocomposites

ZrO_2-C_{60} nanocomposites, showed more photocatalytic effect than unheated nanomaterials in the degradation of organic dyes *i.e.*, methylene blue, methyl orange and rhodamine-B.

Fig. 3 showed XRD patterns of the unheated ZrO_2 nanoparticles, heated ZrO_2 nanoparticles, unheated ZrO_2-C_{60} nanocomposites and heated ZrO_2-C_{60} nanocomposites. Unheated ZrO_2 nanoparticles showed no particular peaks because of their amorphous states [Fig. 3(a)]. After heat treatment, heated ZrO_2 nanoparticles showed their significant peaks. The locations of heated ZrO_2 nanoparticles peaks were at approximately 28.32, 34.43, 50.21 and 60.08 as a 2θ shown in Fig. 3(b). The locations of the peaks were similar in the unheated ZrO_2-C_{60} nanocomposites and heated ZrO_2-C_{60} nanocomposites. On the other hand, the intensity of some peaks were changed; when we observed at the peak of C_{60}, the unheated ZrO_2-C_{60} nanocomposites have higher peaks than the heated ZrO_2-C_{60} nanocomposites due to crush C_{60} nanoparticles after the heat treatment at 700 ºC for 2 h. The XRD patterns due to the C_{60} species in the unheated ZrO_2-C_{60} nanocomposies showed peaks at approximately 10.80, 17.73, 20.78, 21.71, 27.50, 28.15, 32.77 and 33.56 as a 2θ shown in Fig. 3(c). In addition, the peak of C_{60} in the heated ZrO_2-C_{60} nanocomposites showed peaks at approximately 10.83, 17.77, 20.82, 21.69, 27.45, 28.15, 32.88 and 35.06 as a 2θ shown in Fig. 3(d).

Fig. 4 showed UV-visible spectra of the degraded organic dyes (MB, MO and RhB) with unheated ZrO_2 nanoparticles, heated ZrO_2 nanoparticles, unheated ZrO_2-C_{60} nanocomposites and heated ZrO_2-C_{60} nanocomposites under ultra-violet irradiation at 254 nm for 20 min. Figs. 4.1-4.4. showed the UV-visible spectra of the degradation of (a) methylene blue, (b) methyl orange and (c) rhodamine-B on the unheated ZrO_2 nanoparticles, heated ZrO_2 nanoparticles, unheated ZrO_2-C_{60}

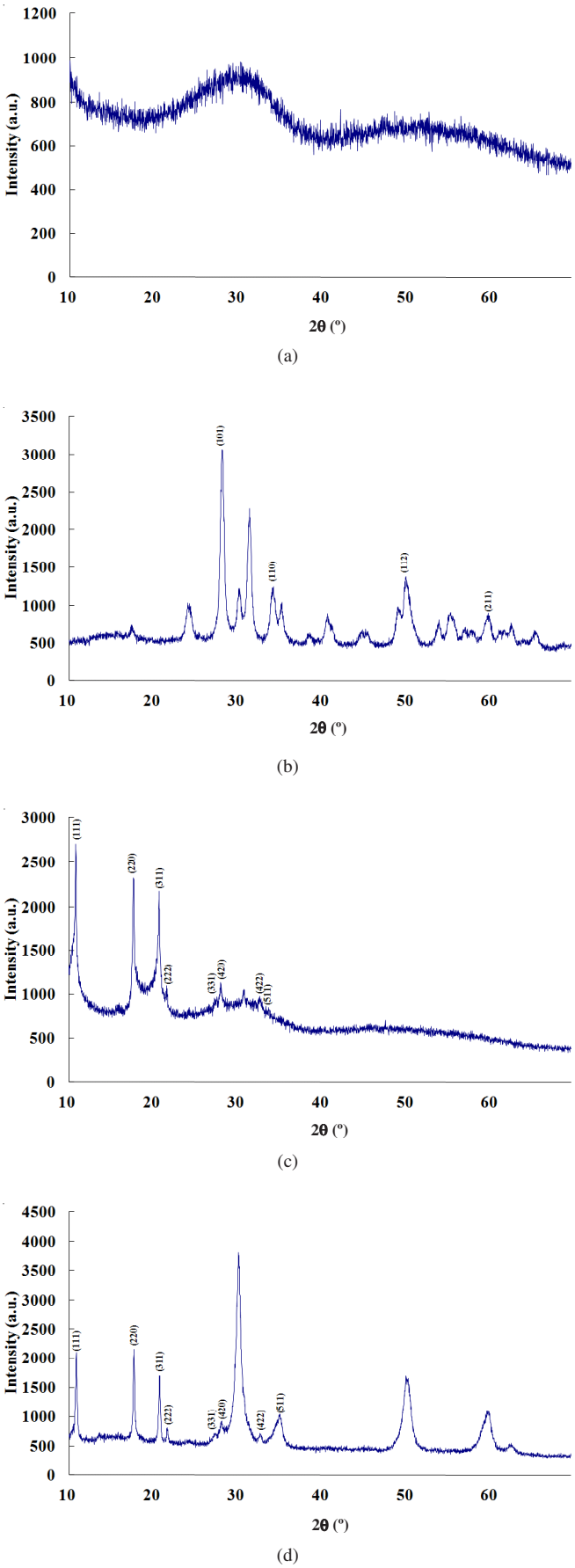

Fig. 3. XRD images of (a) unheated ZrO_2 nanoparticles, (b) heated ZrO_2 nanoparticles, (c) unheated ZrO_2-C_{60} nanocomposites, and (d) heated ZrO_2-C_{60} nanocomposites

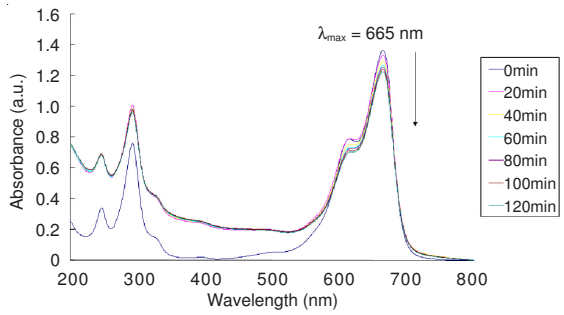

(a)

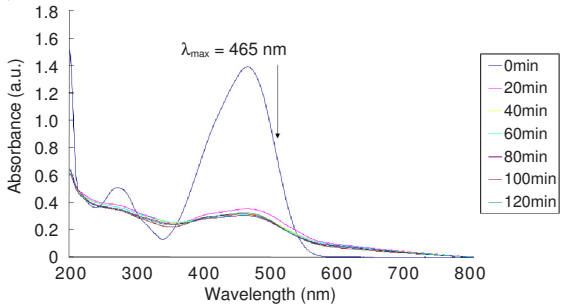

(b)

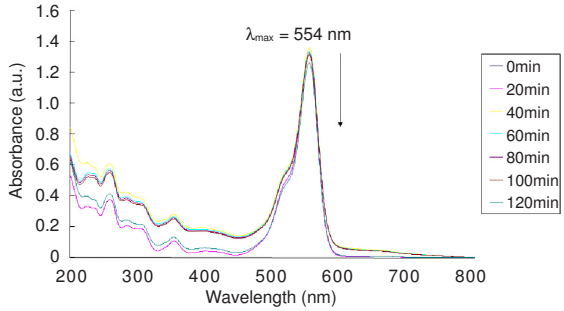

(c)

Fig. 4.1. UV-visible spectra of the degradation in (a) methylene blue, (b) methyl orange, and (c) rhodamine-B with unheated ZrO_2 nanoparticles

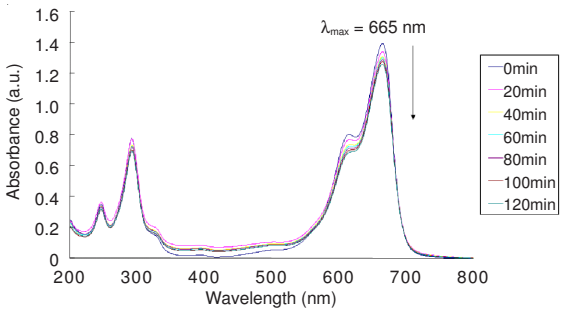

(a)

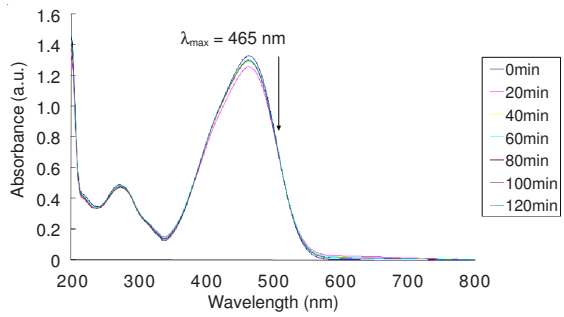

(b)

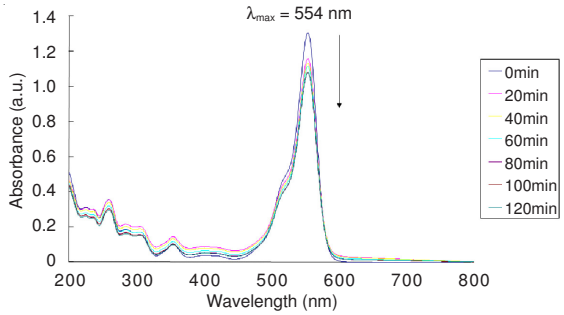

(c)

Fig. 4.2. UV-visible spectra of the degradation in (a) methylene blue, (b) methyl orange, and (c) rhodamine-B with heated ZrO_2 nanoparticles

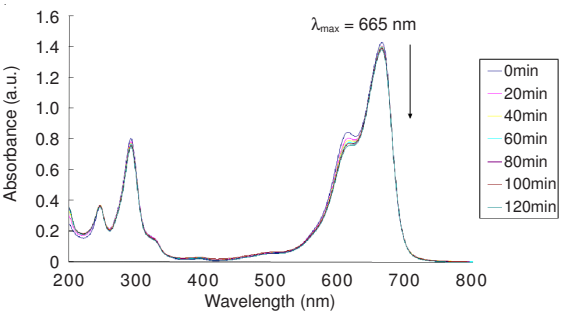

(a)

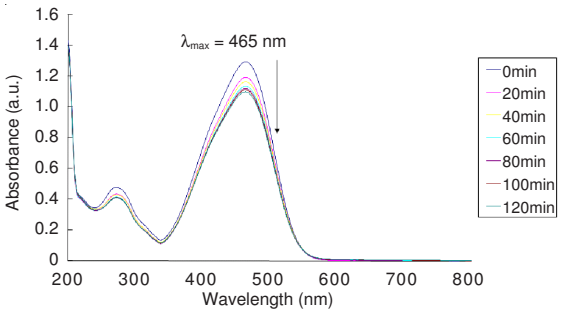

(b)

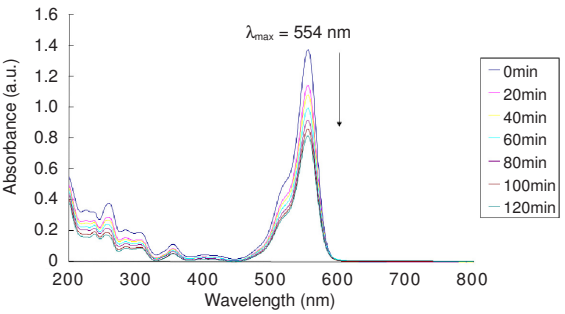

(c)

Fig. 4.3. UV-visible spectra of the degradation in (a) methylene blue, (b) methyl orange, and (c) rhodamine-B with unheated ZrO_2-C_{60} nanocomposites

nanocomposites and heated ZrO_2-C_{60} nanocomposites, respectively. Fig. 4.1(a) and 4.2(a) showed unheated ZrO_2 and heated ZrO_2 nanoparticles had similar efficiencies to degrade in methylene blue. Compared unheated ZrO_2 with heated ZrO_2 nanoparticles, the unheated ZrO_2 nanoparticles showed in Fig. 4.1(b) had rapidly dropped its peak line after 20 min because

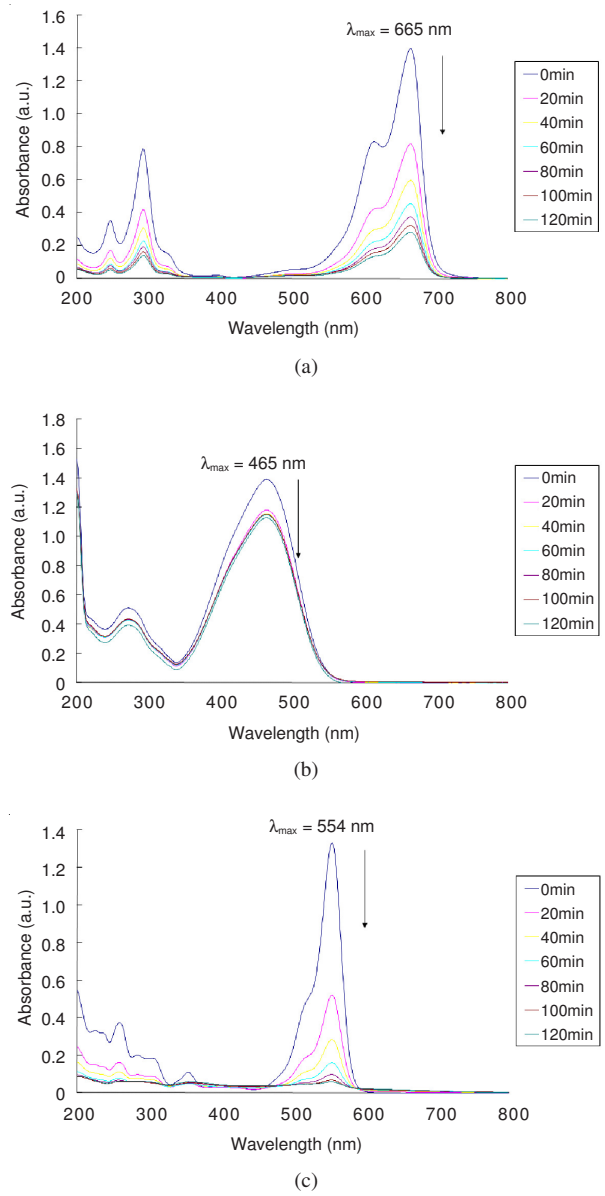

Fig. 4.4. UV-visible spectra of the degradation in (a) methylene blue, (b) methyl orange and (c) rhodamine-B with heated ZrO_2-C_{60} nanocomposites

the unheated ZrO_2 nanoparticles absorbed the methyl orange but the heated ZrO_2 nanoparticles did not absorb in Fig. 4.2(b). In addition, showed in Fig. 4.1(c) and Fig. 4.2(c), heated ZrO_2 nanoparticles had more effective than unheated ZrO_2 nanoparticles in rhodamine-B. Compared unheated ZrO_2-C_{60} nanocomposites with heated ZrO_2-C_{60} nanocomposites showed in Fig. 4.3. and 4.4, heated ZrO_2-C_{60} nanocomposites were more efficient than unheated ZrO_2-C_{60} nanocomposites in organic dyes which we have considered. Overall, heated ZrO_2-C_{60} nanocomposites showed the most degraded efficiencies for organic dyes such as methylene blue, methyl orange and rhodamine-B.

Conclusion

Unheated ZrO_2 nanoparticles, heated ZrO_2 nanoparticles, unheated ZrO_2-C_{60} nanocomposites and heated ZrO_2-C_{60} nanocomposites were synthesized as a catalyst for the degradation of methylene blue, methyl orange and rhodamine-B under ultra-violet irradiation at 254 nm for 20 min. Unheated ZrO_2 nanoparticles and heated ZrO_2 nanoparticles showed similar agglomerated morphologies but the heated ZrO_2 nanoparticles had smaller particle size than unheated ZrO_2 nanoparticles. C_{60} nanoparticles were broken into small parts in heated ZrO_2-C_{60} nanocompsoites and also the shape of heated ZrO_2-C_{60} nanocomposites had a porous surface after heating at 700 ºC for 2 h. Since the heated nanomaterials showed increased surface areas because their nanoparticles had decomposed at high temperatures, the heated ZrO_2 nanoparticles and heated ZrO_2-C_{60} nanocomposites were more effective in degrading the organic dyes. Overall, heated ZrO_2-C_{60} nanocomposites had better photocatalytic effects in the degradation of organic dyes such as methylene blue, methyl orange and rhodamine B under ultra-violet irradiation at 254 nm than the other nanomaterials.

ACKNOWLEDGEMENTS

This study was supported by Sahmyook University funding in Korea and the Ministry of Knowledge and Economy.

REFERENCES

1. F. Heshmatpour and R.B. Aghakhanpour, *Powder Technol*., **205**, 193 (2011).
2. I. Birkby and R. Stevens, *Key Eng. Mater*., **122**, 527 (1996).
3. J.W. Fergus, *J. Power Source*, **162**, 30 (2006).
4. G.D. Wilk and R.M. Wallace, *Appl. Phys. Lett*., **76**, 112 (2000).
5. E. Dela, L.A. Diaz-Torres Rosa-Cruz, P. Salas, V.M. Castano and J.M. Hernandez, *J. Phys. D*, **34**, 83 (2001).
6. A. Corma, *Chem. Rev*., **95**, 559 (1995).
7. S. Djerad, B. Geiger, F.J.P. Schott and S. Kureti, *Catal. Commun*., **10**, 1103 (2009).
8. B.T. Lee, J.K. Han and F. Saito, *Mater. Lett*., **59**, 355 (2005).
9. S. Shukla, S. Seal, R. Vij and S. Bandyopadhyay, *J. Nanopart. Res*., **4**, 553 (2002).
10. Y. Jia, Y. Hotta, C. Duran, K. Sato and K. Watari, *J. Ceram. Soc. Japan*, **113**, 380 (2005).
11. M. Salavati-Niasari, M. Dadkhah and F. Davar, *Inorg. Chim. Acta*, **362**, 3969 (2009).
12. G.-Y. Guo and Y.-L. Chen, *J. Solid State Chem.*, **178**, 1675 (2005).
13. J. Liang, X. Jiang, G. Liu, Z. Deng, J. Zhuang, F. Li and Y. Li, *Mater. Res. Bull*., **38**, 161 (2003).
14. V.A. Sadykov, V.I. Zaikovskii, D.A. Zyuzin, E.M. Moroz, E.B. Burgina and A.V. Ishchenko, *Mater. Res. Soc. Symp. Proc. E*, **878**, 481 (2005).
15. V. Apostolopoulou, J. Vakros, C. Kordulis and A. Lycourghiotis, *Colloids Surf*., **349**, 189 (2009).
16. J.W. Arbogast, A.P. Darmanyan, C.S. Foote, Y. Rubin, F.N. Diederich, M.M. Alvarez, S.J. Anz and R.L. Whetten, *J. Phys. Chem*., **95**, 11 (1991).
17. M. Terazima, N. Hirota, H. Shinohara and Y. Saito, *J. Phys. Chem*., **95**, 9080 (1991).
18. M. Orfanopoulos and S. Kambourakis, *Tetrahedron Lett*., **35**, 1945 (1994).
19. H. Tokuyama and E. Nakamura, *J. Org. Chem*., **59**, 1135 (1994).
20. M. Orfanopoulos and S. Kambourkis, *Tetrahedron Lett*., **36**, 435 (1995).
21. W. Krätschmer, L.D. Lamb, K. Fostiropoulos and D.R. Huffman, *Nature*, **347**, 354 (1990).
22. H. Ajie, M.M. Alvarez, S.J. Anz, R.D. Beck, F. Diederich, K. Fostiropoulos, D.R. Huffman, W. Krätschmer, Y. Rubin, K.E. Schriver, D. Sensharma and R.L. Whetten, *J. Phys. Chem*., **94**, 8630 (1990).
23. W. Krätschmer, K. Fostiropoulos and D.R. Huffman, *Chem. Phys. Lett*., **170**, 167 (1990).
24. T.W. Ebbesen, K. Tanigaki and S. Kuroshima, *Chem. Phys. Lett*., **181**, 501 (1991).
25. M.R. Fraelich and R.B. Weisman, *J. Phys. Chem*., **97**, 11145 (1993).
26. Y. Kajii, T. Nakagawa, S. Suzuki, Y. Achiba, K. Obi and K. Shibuya, *Chem. Phys. Lett*., **181**, 100 (1991).
27. Q. Xie, E. Perez-Cordero and L. Echegoyen, *J. Am. Chem. Soc*., **114**, 3978 (1992).

28. Y. Ohsawa and T. Saji, *J. Chem. Soc. Chem. Commun*., 781 (1992).
29. J.H. Lee, S.K. Hong and W.B. Ko, *J. Korean Ind. Eng. Chem*., **16**, 564 (2010).
30. U. Kreibig and L. Ganzel, *Surf. Sci*., **156**, 678 (1985).
31. A. Henglein, *Chem. Rev*., **89**, 1861 (1989).
32. M.D. Morse, *Chem. Rev*., **86**, 1049 (1986).
33. A. Inoue and B.L. Shen, *Chem. Rev*., **86**, 1049 (1986).
34. S. Krongelb, L.T. Romankiw and J.A. Tornello, *IBM J. Res. Dev*., **42**, 575 (1998).
35. T. Mitsuyu, O. Yamakazi, K. Ohji and K. Wasa, *Ferroelectrics*, **42**, 233 (1982).
36. Y. Jiang, S. Decker, C. Mohs and K.J. Klabunde, *J. Catal*., **180**, 24 (1998).
37. U. Bjoerksten, J. Moser and M. Graetze, *Chem. Mater*., **6**, 858 (1994).
38. J. Tamaki, K. Shimanoe, Y. Yamada, Y. Yamamoto, N. Miura and N. Yamazoe, *Sens. Actuators B*, **49**, 121 (1998).
39. M.M. Viitanen, W.P.A. Jansen, R.G. Welzenis, H.H. Brongersma, D.S. Brands, E.K. Poels and A. Bliek, *J. Phys. Chem. B*, **103**, 6025 (1999).
40. W.P. Dow and T.J. Huang, *J. Catal*., **160**, 171 (1996).
41. S. Farhadi and M. Zaidi, *Appl. Catal. A: Gen.*, **354**, 119 (2009).
42. T. Mallat and A. Baiker, *Chem. Rev*., **104**, 3037 (2004).
43. N. Jiang and A.J. Ragauskas, *Tetrahedron Lett*., **48**, 273 (2007).
44. A. Maldotti, R. Molinari and A. Amadelli, *Chem. Rev*., **102**, 3811 (2002).
45. J. Fenoll, P. Hellin, C. M. Martinez, P. Flores and S. Navarro, *Appl. Catal. B: Environ*., **115**, 31 (2012).
46. I.K. Konstantinou and T.A. Albanis, *Appl. Catal. B*, **92**, 311 (2003).
47. P. Pichat, S. Vannier, J. Dussaud and J.P. Rubis, *Sol. Energy*, **77**, 533 (2004).
48. S.K. Hong, G.Y. Yu, C.S. Lim and W.B. Ko, *Elast. Compos*., **45**, 206 (2010).